# Chapter 5

# Magnetic properties of ultrathin Ho films

The technique of molecular-beam epitaxy allows the fabrication of well-defined thin films on a substrate, and also superlattices or multilayers can be grown with high quality. Hence, this technique opened up the field of thin-film magnetism and gave access to systematic studies of low-dimensional magnetic systems.

The essential differences between thin films and bulk crystals are due to the boundary conditions and the reduced dimension in one direction. Films are finite in one direction and essentially infinite in the other two, whereas a bulk crystal is assumed to be unbound or at least semi-infinite. Thus, when comparing the results from epitaxially grown films to those obtained from bulk samples, one has to be aware of the fact that the structural and magnetic properties may be different. The cause for these differences can be intrinsic, like the broken symmetry or the reduced dimension, or they can be induced by substrate or interfaces properties. The influence of surfaces and interfaces becomes increasingly important when the film thickness is reduced. In this respect, the most interesting range is that where the magnetic structure and magnetic properties are strongly altered by the finite thickness of the film, and where a dimensional crossover may occur. While most studies in this thickness range have focused on FM $3d$ transition-metal films, comparably little is known about local-magnetic-moment systems like lanthanide-metal films and almost nothing about finite-size effects in AFM systems (see discussion in section 1.3). Since Ho is a long-period antiferromagnet in a large temperature interval with a well-known bulk magnetic structure, it is a promising prototypical system to advance in this thickness range. With the huge resonant enhancement of the magnetic-scattering signal at the $M_V$ absorption threshold of Ho, a direct probe of the magnetic structure is available for ultrathin films that works well down to the thickness range corresponding to the period length of the helical structure.

The first part of this chapter deals with the thickness and temperature dependence of the magnetic structure in ultrathin Ho films and with the influence of interfaces and surfaces. The influence of the film thickness on the ordering temperature and the dimensionality of the phase transition are discussed in the second and third part, respectively.

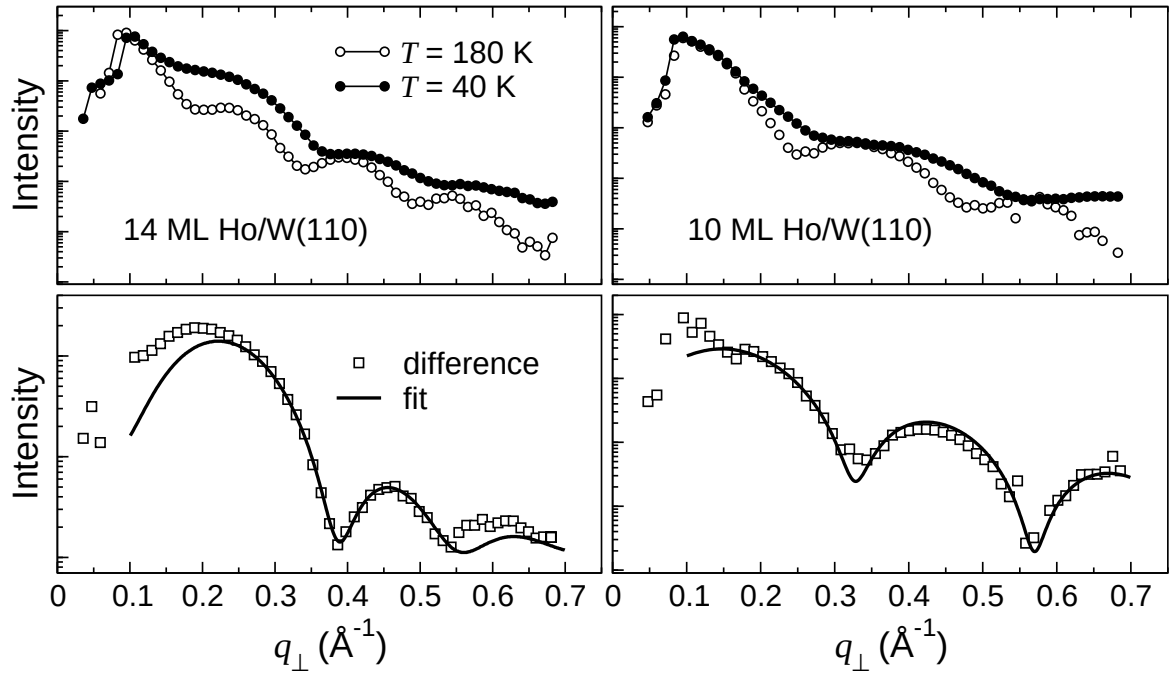


**Figure 5.1:** Reflectivity curves from ultrathin Ho-metal films grown on W(110), recorded at the maximum of the $M_V$ resonance. The upper panels show the reflectivity scans of a 14-ML (left) and a 10-ML (right) film measured at 40 K in the magnetically ordered phase (filled circles) and at 180 K in the paramagnetic phase (open circles). In the lower panels, the corresponding difference spectra are displayed, representing the magnetic scattering contribution. The solid lines are the results of least-squares fit analyses according to a dynamical model using a single magnetic modulation vector.

## 5.1 Magnetic structure

Even though magnetic scattering in the soft x-ray regin is well suited to study long-period AFM structures and the scattering cross section at the $M_V$ resonance is huge, the study of thin films is not an easy task. As discussed in the previous chapters, the diffraction signal of a thin film does not consist of a single sharp peak, but is strongly broadened (cf. equation 2.6), and sits on a structured charge-scattering background formed by the Kiessig fringes, which makes it difficult to separate magnetic and charge scattering from thin films. This is demonstrated in figure 5.1 for a 14-ML and 10-ML Ho film grown on W(110). The upper panels display the diffraction signals as recorded at temperatures of 40 K in the magnetically ordered phase (filled circles) and of 180 K well above the ordering temperature (open circles). Since at 180 K the long-range magnetic structure does not exist any more, the additional intensity at 40 K must be due to magnetic scattering. The simplest approach to separate the magnetic signal is to take the difference of the two curves, assuming that magnetic-charge interference is negligible. The difference spectra are displayed in the respective lower panels of figure 5.1. In both cases, the difference

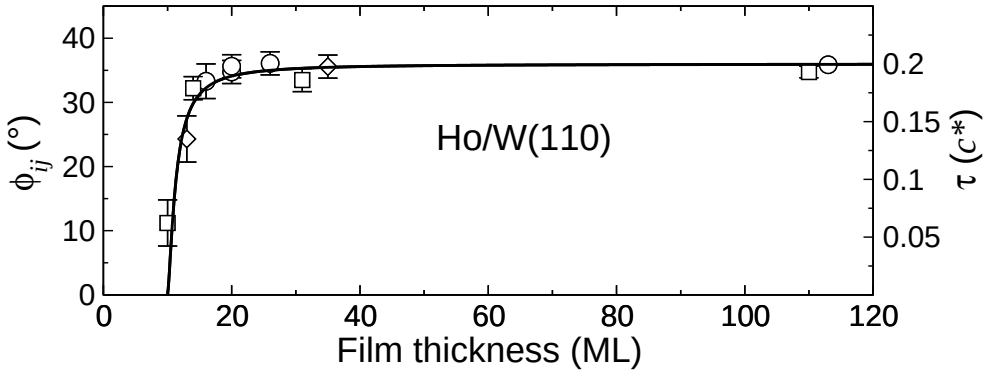


**Figure 5.2:** Magnetic modulation vector and turning angle between the magnetic moments of adjacent atomic planes for films of different thicknesses grown on W(110). The solid line through the data points serves as a guide to the eyes.

spectra reveal a magnetic-superstructure satellite with well-pronounced side maxima and minima. The simplest option to extract the magnetic modulation vector is provided by the position of the main diffraction peak. Even when the peak maximum is not well defined, as in case of the 10-ML film, the positions of the side maxima and minima already contain the information on the magnetic period. A second approach for the analysis is given by the fit model as described in the previous chapter, assuming further that the helical AFM structure with a uniform turning angle between magnetic moments in neighboring planes persists in ultrathin films, which is not necessarily the case. And in fact, a fit on a logarithmic scale, emphasizing a proper description of the Laue oscillations, deviates appreciable from the data points near the main maximum of the diffraction peak (solid lines in the lower panels of figure 5.1). This systematic deviation of the fit from the experimental data is particularly obvious in case of the 14-ML film. However, comparing the two different methods gives an estimate of the error bars, and the magnetic modulation vector of the 14-ML Ho film is determined to be $\tau/c^* = 0.18 \pm 0.01$; this means that only 1.3 magnetic periods exist in the film. While the period of the 14-ML Ho film is nearly bulk-like, a drastic change of the period is found for thinner films. The analysis of the 10-ML film on the right side of figure 5.1 yields a magnetic period of $\tau/c^* = 0.06 \pm 0.02$ corresponding to a helix period of about 29 monolayers, which means that only one third of a period is present in this film. This longer period length corresponds to a smaller angle between moments in adjacent layers and hence to a tendency towards a FM alignment. The systematic change of the magnetic modulation vector and the turning angle of magnetic moments of adjacent atomic planes as a function of the film thickness is displayed in figure 5.2. The abrupt decrease of the modulation vector around 14 monolayers indicates that a FM alignment in Ho films below a thickness of 9 monolayers is favored. This result is in perfect agreement with calculations of Bohr *et al.*, which predicted a transition to FM order around a thickness of 9 monolayers [63]. With the sensitivity of resonant magnetic scattering, this could be verified experimentally for the first time in the present work.

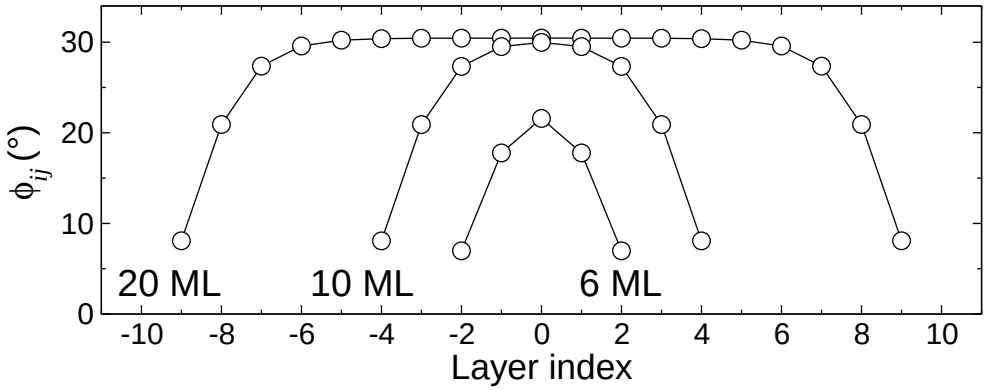


**Figure 5.3:** Results of mean-field calculations using fixed exchange coupling constants $J_0 - J_2$ for various thicknesses at $T = 0$ K. $\phi_{ij}$ denotes the angle between the magnetic moments of adjacent planes. Note the tendency towards FM order, i.e. a smaller angle, at the outermost layers.

Motivated by this experimental result, Peter Jensen[1] carried out mean-field calculations using a Heisenberg Hamiltonian. The simplest model, which reproduces the magnetic structure of Ho, considers three exchange parameters $J_0$, $J_1$, and $J_2$. $J_0 > 0$ accounts for the FM coupling of the $4f$ spins within the basal planes, while $J_1$ and $J_2$ describe the coupling between the nearest and next-nearest planes. For an infinite system at $T = 0$ K, $J_1 > 0$ and $J_2 < 0$ lead to a homogeneous helical structure with a constant angle $\phi_{ij} = \phi$ between the moments of adjacent FM planes described by $\cos\phi = -J_1/4J_2$, provided that $|J_1/4J_2| < 1$. The parameter set $J_0 = 330\mu$eV, $J_1 = 100\mu$eV, and $J_2 = -29\mu$eV reproduces the bulk properties of Ho metal: a temperature-dependent calculation leads to the bulk Néel temperature of $T_N = 132$ K and a helix with a turning angle of $\phi = 30.5°$.

For films of finite thickness it turns out that only the inner film layers exhibit a constant turning angle like in the infinite system. At the surface, however, the relative weight of the AFM next nearest interlayer coupling $J_2$ is reduced with respect to the FM interlayer coupling $J_1$, resulting in a smaller angle $\phi_{ij}$ in the surface region. The calculated turning angles as a function of the layer index are displayed for three film thicknesses in figure 5.3. Thick films are characterized by an inner region with constant turning angle (12 layers in case of the 20-ML film), while the turning angle decreases strongly in a surface region of 4 ML thickness. With decreasing film thickness, the surface regions get increasingly important, which means that a helical AFM structure is no longer well defined below a film thickness equal to two times the thickness of the distorted surface region. A ferromagnetic alignment of all moments is favored below a film thickness of 5 monolayers. With this theoretical insight on relevant details of the magnetic structure, one can try to analyze the thin-film magnetic signal in more detail. The results of the analysis are shown in figure 5.4. The solid lines through the data points in both spectra represent fits with an extended

[1]Peter J. Jensen, Freie Universität Berlin, Department of Physics, Arnimallee 14, 14195 Berlin, Germany, e-mail: jensen@physik.fu-berlin.de

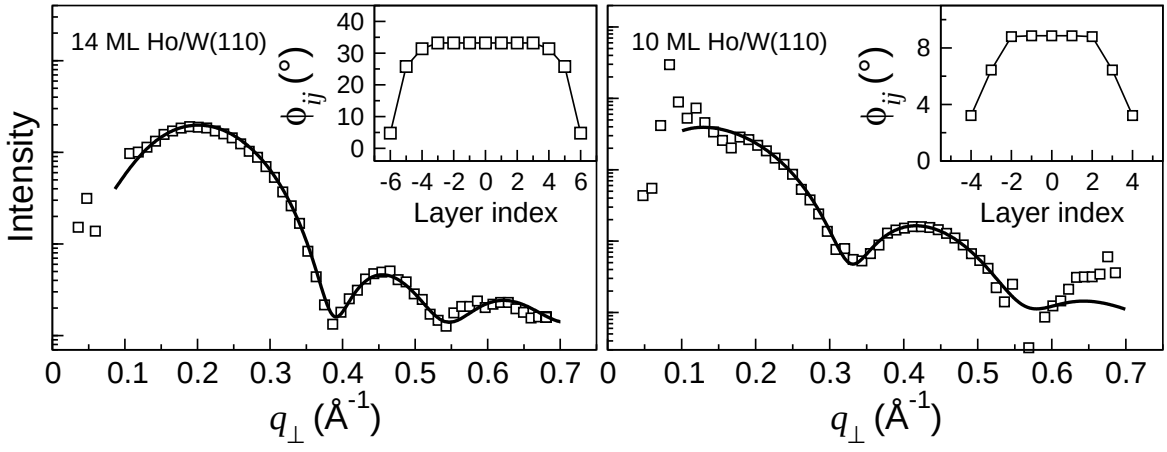


**Figure 5.4:** Difference spectra from figure 5.1, representing the magnetic contribution of a 14-ML (left panel) and 10-ML (right panel) film. The solid lines through the data points represent fits with a magnetic profile as displayed in the respective insets.

version of the model introduced in section 4.1. In addition to the previous analysis, the turning angles between the three outermost monolayers adjacent to the interface and to the surface were varied in order to achieve a reasonable description of the spectra. The obtained magnetic profiles are shown in the respective insets of figure 5.4. Leaving these parameters completely free, gave unreasonable results. Therefore, the result does not correspond to the best fit if the turning angles were treated as free parameters. It is, however, a rather reasonable model, which describes details of the spectra that are not covered when a single modulation vector is used. When we take the distortions of the magnetic structure into account, we arrive at results for the mean harmonic modulation period that are different from those plotted in figure 5.2. In the limit of thick films, the deviation from a helix with a single modulation vector is small, and both models give essentially the same number. In ultrathin films, however, the numbers given in figure 5.2 are slightly smaller than the respective turning angles between inner layers, when the more complex magnetic profile is taken into account. This, however, does not change the general picture, since the improved values are within the error bars of the data points in figure 5.2.

In contrast to the films grown on W(110), which exhibit a tendency towards FM order, a behavior with the opposite trend is found for Ho films embedded between Y layers. In those films, the angles between moments of adjacent planes tend to a 'more antiferromagnetic' alignment with a larger magnetic modulation vector in thin films, while in the limit of thick films, both types of samples show comparable magnetic periods. A comparison of the thickness dependence of Y-bound Ho films to that of Ho films grown on W(110) is displayed in figure 5.5. Evidently, this opposite behavior is caused by the respective interfaces. While a tendency to larger modulation vectors has also been found for Ho/Y superlattices [125], the underlying mechanism is still a matter of discussion. One possible cause is the lattice mismatch at the Ho/Y interface of about 2 percent that may stabilize the AFM structure in Ho. The mechanical stress due to this mismatch is highly anisotropic: the crystalline

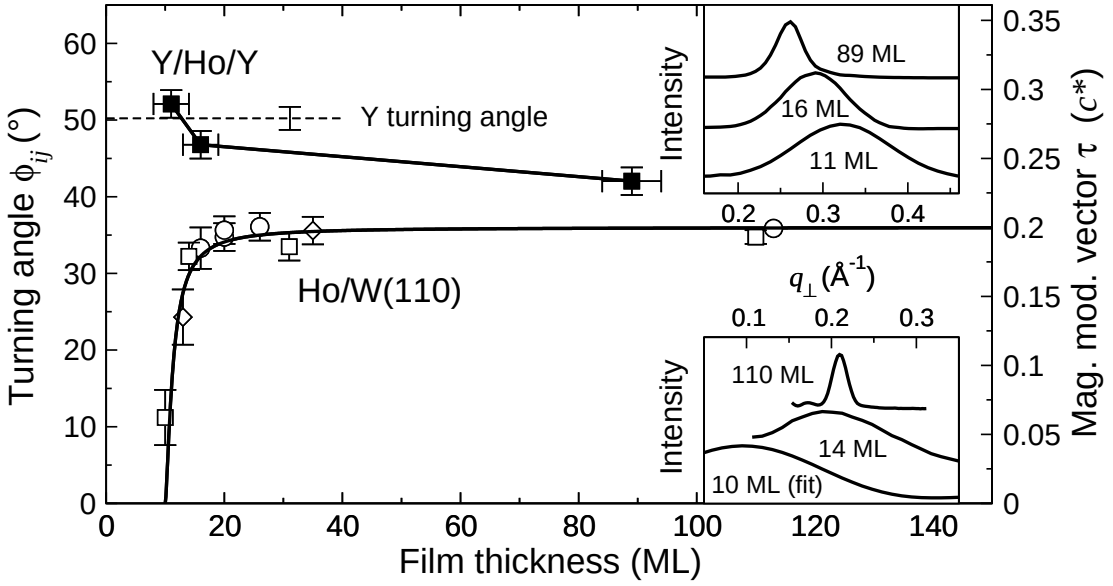


**Figure 5.5:** Thickness dependence of the magnetic modulation vector and the respective turning angle between magnetic moments in adjacent atomic planes. The data are obtained from Ho films embedded between Y layers (filled symbols) and Ho films grown on W(110) (open symbols) at 40 K. The solid lines through the data points serve as a guide to the eyes. The value of the Y turning angle has been taken from reference 125. The insets show corresponding raw data. The spectra are vertically offset for clarity.

lattice of Ho is expanded in the basal plane, but contracted along the $c-$axis, which leads to a modification of magnetic coupling. This strain is supposed to be responsible for the suppression of the low-temperature cone phase and also for the change in the ordering temperature and the low-temperature modulation vector in Ho/Y superlattices [125].

There is another mechanism that can be considered. The ability of the conduction electrons to establish a magnetic structure depends strongly on the topology of the Fermi surface. Like in many of the heavier lanthanide metals, the Fermi surface of Y metal shows a nesting feature [36, 37] (the Fermi-surface of Y is displayed in figure 1.1). This enables Y to mediate an AFM coupling between magnetic ions, e.g. in case of Gd-Y alloys [37]. A reduced film thickness leads to an increasing influence of the interface properties. It is thus plausible that in a Ho film of only a few monolayers thickness the magnetic coupling is dominated by the electronic structure of the surrounding Y. The experimental data of the present work supports this possibility due to the systematic approach of the magnetic modulation vector towards a value close to the nesting vector of Y for the thinnest films: The nearly temperature-independent turning angle of Y (50.2°±1.5°), as found in Ho/Y superlattices, is displayed as the dashed line in figure 5.5. The stability of the Y turning angle in the thinner Ho films is reflected in the temperature dependence of the longitudinal scans in figure 5.6. The magnetic-peak position of the 89-ML film shows a bulk-like temperature dependence, whereas it is nearly temperature independent in case of

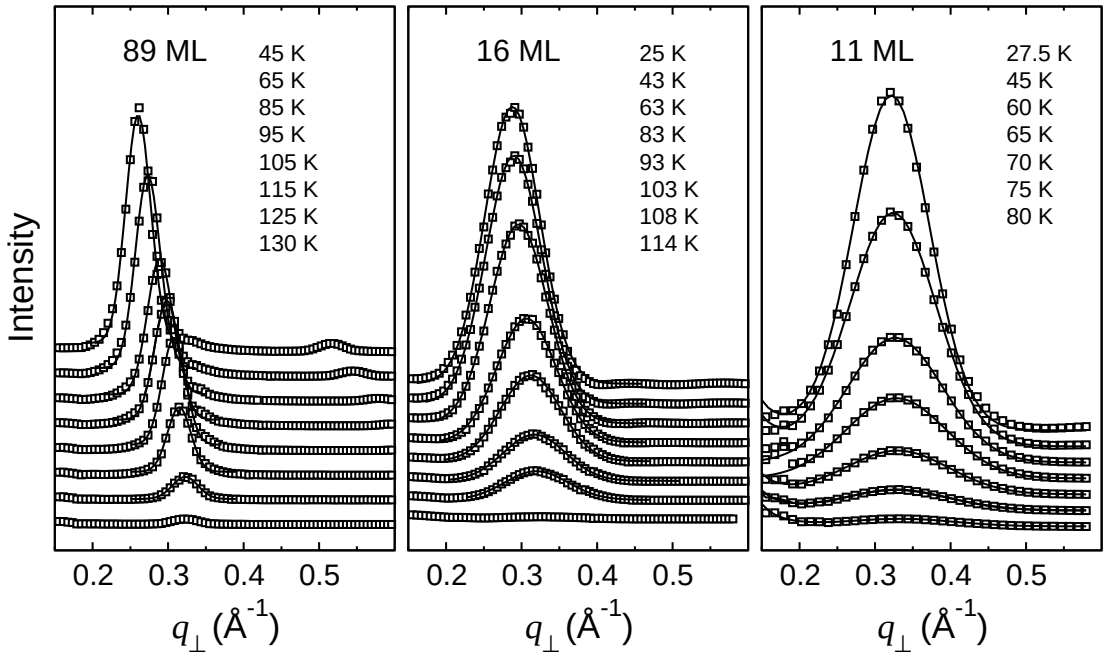


**Figure 5.6:** Magnetic scattering from Ho films embedded between Y layers. The raw data were measured from an 89-ML (left), a 16-ML (middle) and an 11-ML (right) film at various temperatures in specular geometry. In the figure, the spectra are vertically offset for clarity.

the 11-ML film, and appears to be locked in an 'Y-like' magnetic structure.

## 5.2 Reduced magnetic ordering temperature

The lowering of the magnetic ordering temperature in FM thin films is a well-known phenomenon. This finite-size effect is caused by the decrease of the total magnetic exchange energy due to the reduced number of atomic layers. The thickness dependence of the ordering temperature of FM systems can be described by a universal scaling law [21–23]

$$\frac{T_C(\infty) - T_C(d)}{T_C(\infty)} = b \cdot d^{-\lambda}, \tag{5.1}$$

where $T_C(d)$ is the critical temperature of the FM film with finite thickness $d$, and $T_C(\infty)$ the critical temperature of the respective infinite system. The shift exponent $\lambda$ is given by $\lambda = 1/\nu_{3D}$, where $\nu_{3D}$ is the critical exponent describing the magnetic correlation length of the respective three-dimensional system. Besides the scaling hypothesis, the derivation of equation 5.1 is based on the assumption of a homogenous and continuous system neglecting the atomic layer structure, and relatively large $d$ that lead to only small deviations from

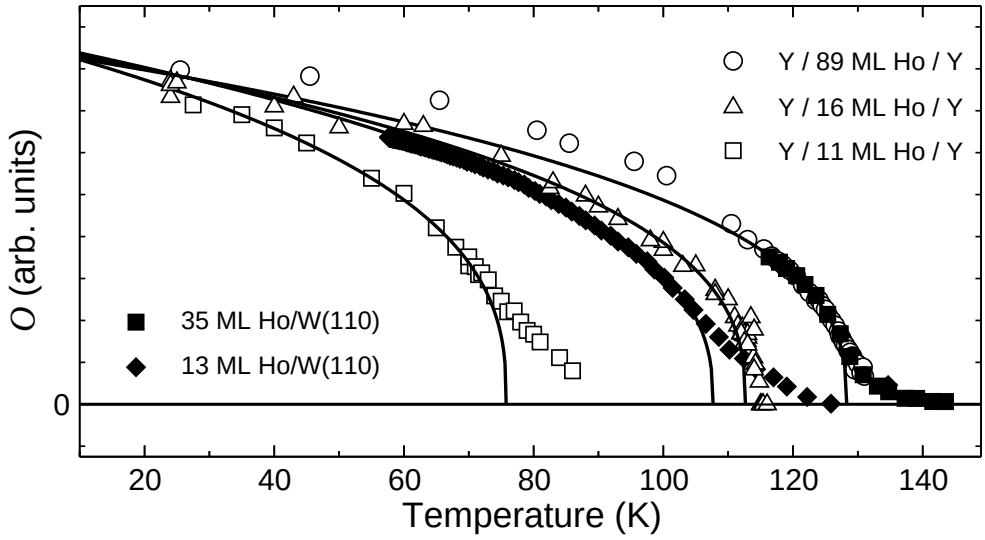


**Figure 5.7:** Temperature dependence of the square roots of the integrated intensities (order parameter $O$) obtained from the $(000{+}\tau)$ magnetic-superstructure satellites of Ho-metal films with different thicknesses and different boundaries. The solid lines through the data points represent power-law fits. Details of the analysis are discussed in section 5.3.

$T_C(\infty)$. Alternatively, the experimental data can be described well by the modified law

$$\frac{T_C(\infty) - T_C(d)}{T_C(d)} = b \cdot d^{-\lambda'}, \tag{5.2}$$

which is generally applicable down to small values of $d$. In general the shift exponent $\lambda'$ in equation 5.2 does not agree with $\lambda$ and is therefore nonuniversal [126, 127]. Reduced ordering temperatures in ferromagnets have been found in many systems, such as Fe [24], Co [25], Ni [26], and Gd [17, 128].

While most of the thin-film studies focused on ferromagnets, little is known about finite-size effects in AFM systems. For one of the few studied systems, the simple antiferromagnet CoO, a finite-size scaling in accordance with equation 5.1 was found [27]. Bulk Ho metal, however, is a long-period helical antiferromagnet with a period length between 7 and 12 monolayers in the temperature interval between $T_N = 131.2$ K and $T_C = 20$ K [6]. In ultrathin films, the magnetic period differs from the bulk and depends strongly on the properties of the boundaries as discussed in the previous section. While the AFM structure is stabilized in ultrathin Y-bound Ho films, Ho films grown on W(110) tend to a FM alignment below $\approx 10$ monolayers. Since an AFM structure can no longer be defined in the latter systems below this thickness, questions concerning the particular finite-size scaling of AFM systems and its dependence on the boundary conditions arise.

Figure 5.6 shows longitudinal scans of an 89-ML (left panel), 16-ML (middle panel), and 11-ML (right panel) film at various temperatures. The different ordering temperatures can already be seen from the respective high-temperature scans. While the magnetic

peak of the 89-ML film is still clearly visible at 125 K and has not even vanished at 130 K, the satellite of the 16-ML film has almost vanished at 114 K, and that of the 11-ML film is already absent around 80 K. In the helical phase, the square root of the magnetic-satellite intensity is proportional to the magnetic order parameter (section 4.3). Hence, the temperature dependence of this quantity can be used to determine the magnetic ordering temperature $T_N$. This is demonstrated in figure 5.7 for both Ho-metal films grown on W(110) (filled symbols) and Y-bound MBE-grown films (open symbols) at various thicknesses. The different temperature scales for the respective magnetic order are clearly visible. The solid lines through the data points represent power-law fits with the 3D-Heisenberg critical exponent $\beta = 0.367$ [123]. The significant deviations of the fits from the experimental data above the obtained ordering temperatures, particularly in case of the thinnest films studied, is due to short-range magnetic correlations that give rise to a finite magnetic satellite intensity in the absence of long-range magnetic order and that occur in a particular large temperature interval in case of ultrathin films. These critical fluctuations are discussed in greater detail in the following section 5.3. Because of these fluctuations, the critical temperatures were determined by a combined analysis of the magnetic correlation lengths above the critical temperatures, and the order parameters below. For $T_N$ we find $75.8 \pm 3$ K, $112.7 \pm 3$ K, and $128.9 \pm 2$ K for the 11-ML, 16-ML, and 89-ML MBE films, respectively.

While the magnetic satellite intensity can be readily determined for the MBE-grown films, the data analysis for films grown on W(110) is slightly more difficult. Due to the smaller magnetic modulation vector in these films, there is a strong overlap of the magnetic satellites with the charge-scattering background. Furthermore, a description with a single magnetic modulation vector is not satisfactory below a certain film thickness (section 5.1). Because of these difficulties, we obtained the ordering temperatures of these films from temperature scans in a fixed specular scattering geometry. This procedure is reliable, since the width of the magnetic satellite is large compared to its shift in the considered temperature range. Hence, the change of the integrated satellite intensity is proportional to the change in intensity measured at a single $q_\perp$ value, if the geometry is chosen such that $q_\perp$ corresponds to the magnetic modulation vector close to the ordering temperature. Although this method is not practicable in the limit of thick films, where the width of the satellite gets very small, and thus a precise knowledge of the peak position at the ordering temperature is required, the method becomes very precise in the limit of ultrathin films, where an approximate position is sufficient to achieve results with small error bars. While a 35-ML Ho-metal film on W(110) (filled squares in figure 5.7) shows a critical temperature close to that of the bulk $127.5 \pm 3$ K, a 13-ML film (filled diamonds) exhibit a clearly reduced ordering temperature of $107.5 \pm 2$ K.

The resulting critical temperatures as a function of the film thickness are summarized in figure 5.8. The results are remarkable in the following respect: despite the very different magnetic structures in the ultrathin-film range, there is no significant difference in the finite-size behavior of the magnetic ordering temperature of both types of samples that are distinguished by squares for the MBE-grown samples and by circles for the samples grown on W(110). For both types of films, $T_N$ goes to zero for thicknesses below $\approx 10$

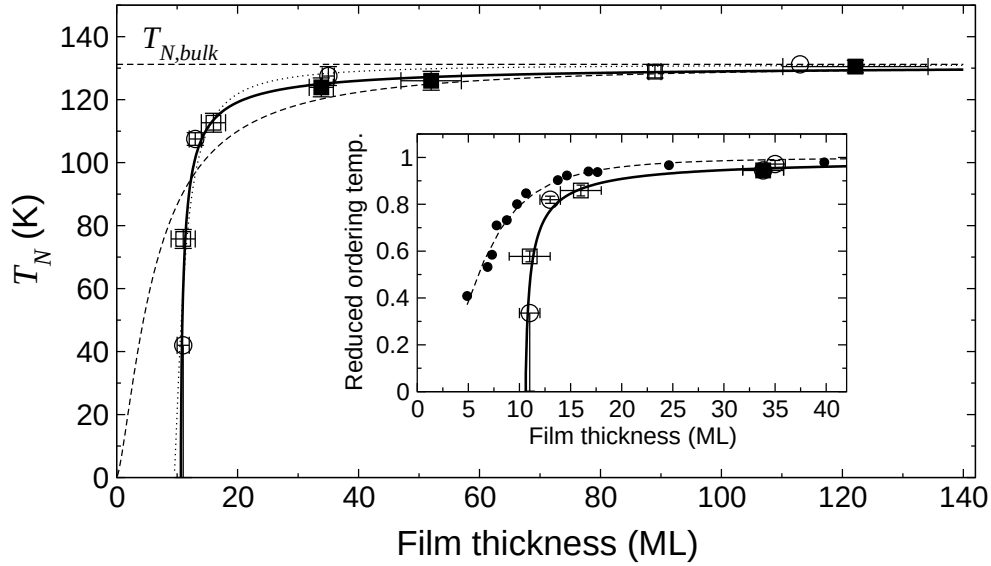


**Figure 5.8:** Néel temperature of Ho films as a function of film thickness. Squares were obtained from Y-bound Ho films, circles from films grown on a W(110) substrate. Open symbols were obtained by resonant soft x-ray scattering, and filled symbols by neutron scattering. The dashed and solid lines represent fits according to equations 5.2 and 5.3, respectively. The inset compares the Ho data to Gd thin-film data (filled circles) measured by Farle *et al.* (from reference 17).

monolayers. The inset compares the Ho data with data from FM Gd metal from reference 17. In contrast to the behavior of the ferromagnet, whose critical temperature $T_C$ goes to zero for zero thickness, the decrease of $T_N$ in Ho-metal films is rather abrupt around a thickness of $\approx 10$ monolayers. Such a behavior can no longer be described by equations 5.1 or 5.2: the best fit of the Ho data by equation 5.2, with the bulk ordering temperature of $T_N = 131.2\,\mathrm{K}$, is shown as a dashed line in the main panel. Although a reasonable number for the critical exponent is obtained, $\lambda = 1.3 \pm 0.3$, similar to the Gd case, the fit curve deviates significantly from the data points for thicknesses smaller than 40 monolayers.

On the other hand a very good description of the data is obtained by an empirical law, introducing an offset thickness $d_0$ [28]:

$$\frac{T_N(\infty) - T_N(d)}{T_N(d)} = b' \cdot (d - d_0)^{-\lambda'} . \tag{5.3}$$

Equation 5.3 had been introduced first to describe the behavior of spin-density waves of Cr-metal in Cr/Fe multilayers [28, 29]. This AFM structure is characterized by a sharp drop of $T_N$ near a Cr-spacer thickness of 50 Å, and by an empirical shift exponent of $\lambda' = 0.8$. While the authors assigned this behavior described by equation 5.3 to spin frustration at the Cr/Fe interfaces in the studied multilayer systems, the observation of a similar behavior in the unfrustrated system Ho rather indicates a general property of long-period antiferromagnets. In fact, the behavior of Ho resembles closely that of Cr metal,

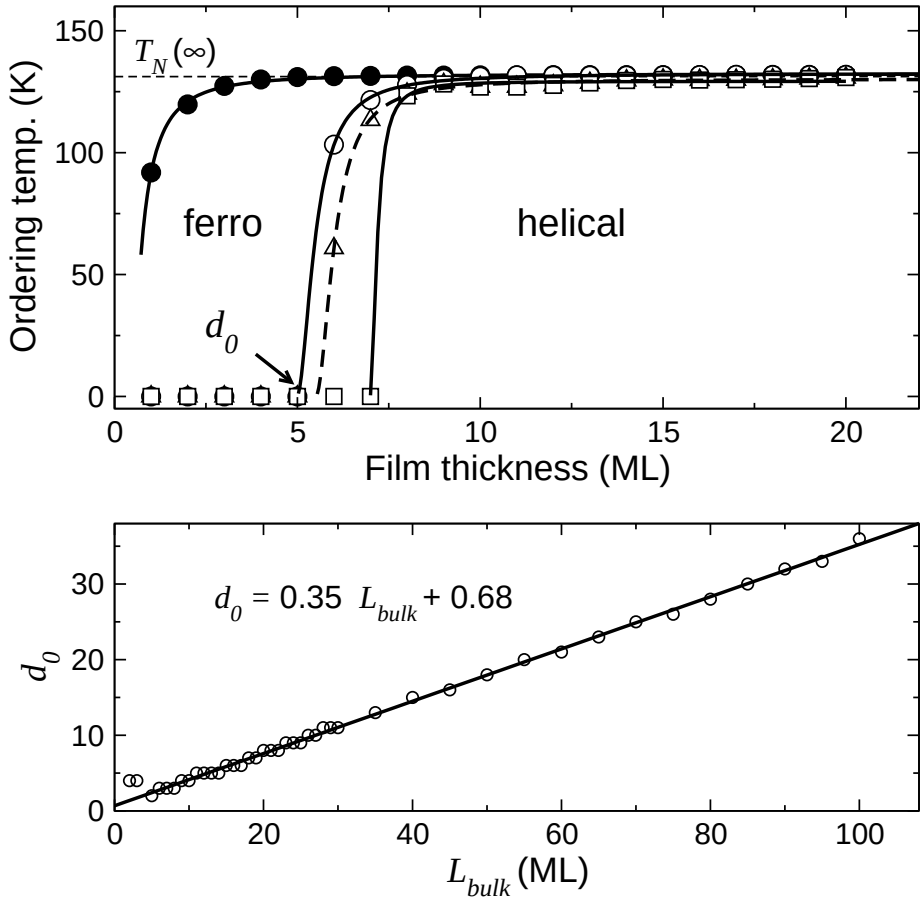


**Figure 5.9:** Upper panel: critical temperature as a function of film thickness, calculated for Ho films within a mean-field model. Two characteristic temperatures have been found corresponding to a transition from the helical AFM to a FM phase (open symbols) and a transition from the FM to the paramagnetic phase (filled symbols). Circles represent the results obtained with a minimum set of exchange parameters $J_0$, $J_1$, and $J_2$. Triangles: extended model using more realistic exchange parameters $J_0$ to $J_6$. Squares: extended model including sixfold hexagonal in-plane anisotropy. Lower panel: critical thickness $d_0$ as a function of the bulk helix period, obtained by variation of the exchange parameters $J_1$ and $J_2$.

with a particularly interesting common feature: $d_0$ is of the same order of magnitude as the period length of the magnetic superstructure in the respective bulk system. A fit of the Ho data according to equation 5.3 is shown as the solid line through the data points in figure 5.3, yielding $\lambda' = 0.86$ and an offset thickness $d_0 = 10.8 \pm 0.5$ monolayers. Also a description with a universal parameter leads to an acceptable description, as given by the dotted line in the main panel of figure 5.3. This represents a fit according to equation 5.3 using the shift exponent of the 3D Heisenberg model, $\lambda = 1.414$. This fit yields essentially the same offset thickness, with $d_0 = 9.9 \pm 0.5$ monolayers.

In order to understand the mechanism underlying the characteristic decrease of $T_N$ in Ho films, mean-field calculations using a Heisenberg Hamiltonian were carried out. The simplest version of the model that already reproduces the helical magnetic structure of Ho considers three exchange parameters $J_0$, $J_1$, and $J_2$, and is discussed for $T = 0$ K in section 5.1. To explore the characteristics of thin films at finite temperatures $T$, the individual angles between magnetic moments of adjacent atomic planes, $\phi_{ij}(T)$, were varied in order to minimize the free energy. The upper panel of figure 5.9 shows the resulting magnetic ordering temperatures as a function of the Ho film thickness $d_{Ho}$. Using the set of parameters $J_0 = 330\,\mu$eV, $J_1 = 100\,\mu$eV, and $J_2 = -29\,\mu$eV, the calculation leads to a helix with a turning angle of $\phi = 30.5°$ and to a magnetic ordering temperature $T_N = 132$K for $d_{Ho} \to \infty$, essentially reproducing the bulk magnetic properties.

At finite $d_{Ho}$, however, a different scenario is found: there are *two* characteristic temperatures. Between the highest magnetic ordering temperature (solid circles in the upper panel of figure 5.9) and a second ordering temperature corresponding to the onset of the helical AFM structure (open symbols), films with $d_{Ho} > 8$ monolayers order in a complex spin-block structure, a non collinear arrangement of blocks of few ferromagnetically aligned layers. For $d_{Ho} \leq 8$ monolayers, this structure is FM; that is why in this case the highest ordering temperature can be denoted by $T_C$. At a second lower temperature $T_N$, the films undergo a smooth transition to an essentially helical structure characterized by finite angles between adjacent ferromagnetically ordered planes, $\phi_{ij}(T)$. For $d_{Ho} \to \infty$, the temperature difference between the two transitions vanishes and at $T_N$ the transition from the paramagnetic directly to the helical AFM phase occurs. Only for $d_{Ho} < 8$ monolayers, the highest ordering temperature and $T_N$ are distinctly different. The thickness dependence of the highest ordering temperature is readily fitted by equation 5.1 (solid line through filled circles), while $T_N(d_{Ho})$ evidently behaves according to equation 5.3 (solid line through the open circles). Fitting the theoretical data yields $\lambda = 1.85$, which is consistent with the mean-field value of $\nu = 0.5$ and $\lambda' = 1.84$.

The particular behavior of $T_N$ with an offset thickness $d_0$ is not a result of the special choice of exchange parameters, but is readily reproduced by various approaches. The open triangles in the upper panel of figure 5.9 represent the results of a calculation using a more realistic set of exchange coupling parameters $J_0$ to $J_6$ as given in reference 63. With these parameters essentially the same behavior is reproduced, in particular the complete suppression of the helical phase below a film thickness of 6 monolayers. Including a crystalline in-plane anisotropy according to the six-fold symmetry of the hcp lattice results in $d_0 = 7$ monolayers (open squares in figure 5.9), thus coming even closer to the experimentally observed value of $d_0 = 10.8$ monolayers. $T_C$ behaves similarly for all models. Considering the simplicity of the theoretical model, theory and experiment are in good agreement.

Both, experiment and mean-field calculations show that $d_0$ is of the same order of magnitude as the period length of the bulk magnetic structure. This close relationship between the bulk magnetic period, $L_{bulk}$, and offset thickness $d_0$ is further established by mean-field calculations. To this end, exchange parameters were varied to yield various values for $L_{bulk}$ according to $\cos\phi = -J_1/4J_2$ (discussed in section 5.1), then $d_0$ was determined numerically using the respective $J_1$ and $J_2$ values. An essentially linear relationship between $d_0$

and $L_{bulk}$ is obtained as displayed in the lower panel of figure 5.9. The numerical value of the slope is a feature of the $J_1 - J_2$ model. The offset thickness may be interpreted as a minimum film thickness, which is required to stabilize the long-period magnetic structure. As these results are qualitatively independent of the special choice of exchange parameters, they can be expected to be generally relevant for a wide class of long-period magnetic structures.

## 5.3 Magnetic critical scattering

An interaction between unpaired magnetic moments in a solid may lead to spontaneous collective long-range magnetic order. As in case of other ordering phenomena, such collective behavior can be described in terms of statistical mechanics. The magnetic order decreases with increasing temperature and vanishes at a *critical temperature* $T_{cr}$, which is specific for the system. Near the transition from order to disorder, the free energy of the system shows a non-analytical behavior leading to singularities in some relevant thermodynamic variables like the *magnetic susceptibility* $\chi(T)$ and the *magnetic correlation length* $\xi(T)$. A central feature of these second-order phase transitions is the appearance of large-scale critical fluctuations. As the critical temperature of a magnetic system is approached, either from below or from above the critical temperature, the size of the region in which the magnetic moments are correlated increases and may become as large as the spatial extension of the magnetic system itself. The average size of the fluctuating domains diverges in an infinite and ideal system as $\xi(T) \propto |T - T_{cr}|^{-\nu}$. Near $T_{cr}$ the behavior of some other variables can be described by power laws as well: the order parameter $O(T) \propto (T_{cr} - T)^{\beta}$ for $T < T_{cr}$ and the susceptibility $\chi(T) \propto |T - T_{cr}|^{-\gamma}$. The dimensionality of a phase transition is reflected in particular values of the critical exponents $\beta, \nu, \ldots$ , which are related to each other by scaling laws. Their values depend only on the spatial dimensionality of the system and the dimensionality of the order parameter, but otherwise they are universal [129].

Magnetic correlation and thus short-range magnetic order in an usually small temperature interval above the critical temperature can be studied by *magnetic critical scattering* [123]. In diffraction, a finite correlation length leads to a broadening of the magnetic Bragg peaks, whose half width at half maximum, $W$, is given by the inverse correlation length, whereas below the critical temperature, in the magnetically ordered phase, $W$ is given by the inverse coherence length of the magnetic structure. Therefore, a precise lineshape analysis of the magnetic diffraction peaks as a function of temperature provides information on the behavior of the correlation length, and in this way on the ordering temperature and the dimensionality of the magnetic system.

Magnetic critical scattering from bulk-Ho metal had been demonstrated first by Thurston *et al.* [130,131]. They found critical fluctuations by means of x-ray and neutron scattering in a temperature interval of about 2 K above the critical temperature. In this temperature interval, the fluctuations exhibit two length scales, indicated by a two-component line shape in all directions of momentum space. The shorter of the two length scales can be described by a Lorentzian and is consistent with 'normal' critical fluctuations, whereas the longer

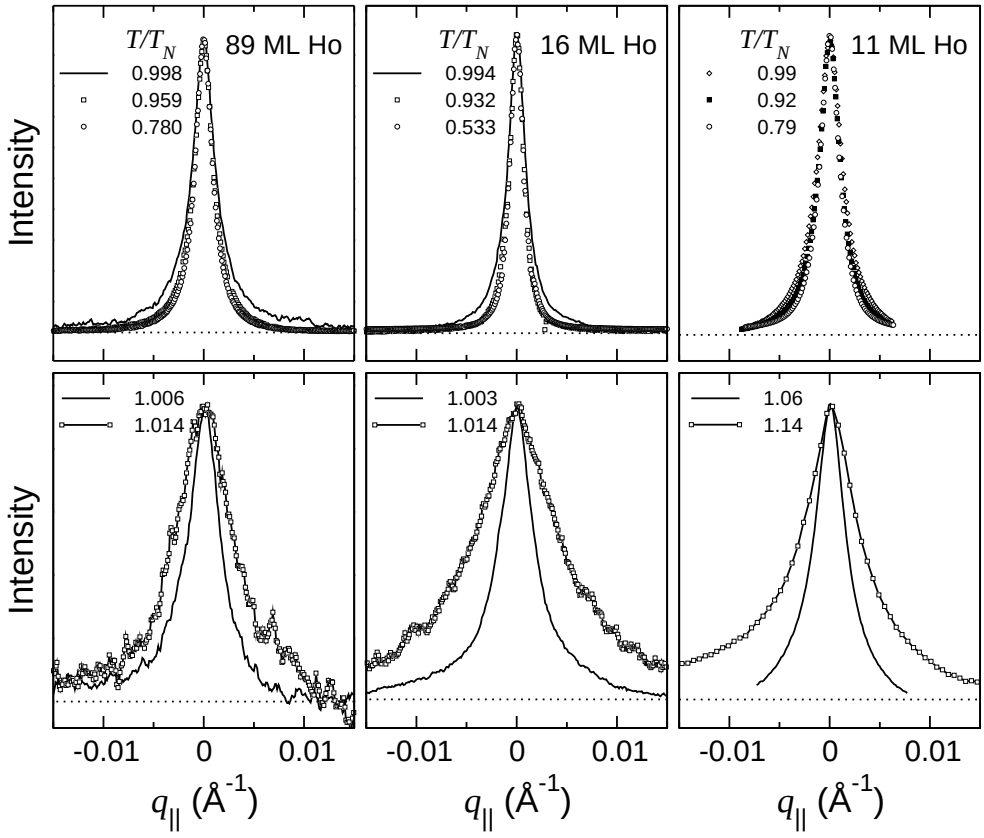


**Figure 5.10:** Transverse scans from 89-ML (left), 16-ML (middle), and 11-ML (right) Ho films taken at the (000+$\tau$) magnetic satellite position. The spectra in the top panels were recorded at temperatures below the magnetic ordering temperatures, the spectra in the lower panels above. The width of the scans is proportional to the inverse magnetic coherence or correlation length.

length scale, which was explained by random strain fields arising from defects localized in a several-micrometer-thick region near the sample surface, can be described by a squared Lorentzian line shape. The correlation lengths of both length scales follow simple power laws above the critical temperature. Below the critical temperature, the diffraction peaks show a constant width representing the mosaic spread of the sample, which is a measure of disorder present in the region of the sample probed by the respective scattering technique. Two component line shapes above the highest ordering temperature have also been found in other experiments on bulk Ho and Tb [73, 132, 133].

Figure 5.10 shows critical scattering data measured from thin Ho-metal films. The transverse scans were taken from an 89-ML, 16-ML, and an 11-ML film below (upper panels) and above (lower panels) the Néel temperature $T_N$. In the whole temperature range and for all samples, the data are perfectly described by a single Lorentzian line shape corresponding to an exponential decay of the magnetic coherence or correlation, respectively. No indications for a second length scale were found. The half-width at half-

maximum (HWHM) of the Lorentzian, $W_{q,\parallel}$, is related to the inverse magnetic correlation or coherence length in the critical region or in the region of long-range magnetic order, respectively: $W_{q,\parallel} = 1/\xi$.

The temperature dependences of $W_{q,\parallel}$ obtained from the transverse scans of the 89-ML and 11-ML films are plotted in figure 5.11 (open circles) together with the square root of the respective integrated satellite intensity, which is proportional to the magnetic order parameter $O$ (for simplicity, in the absence of long-range magnetic order, this quantity will also be denoted as $O$ in the following). Over a large temperature interval below the phase transition, the widths of the transverse scans remain constant corresponding to a constant coherence length of long-range magnetic order. The increasing width above $\approx 126$ K in case of the 89-ML film and 65 K in case of the 11-ML film indicates the presence of short-range magnetic correlation and thus the occurrence of a critical phase transition. Also, the square root of the integrated satellite intensity $O$ shows both characteristic regions. Below the critical temperature $T_N$, in the presence of long-range magnetic order, $O$ shows a power-law behavior followed by a region of a more gradual decay indicating short-range magnetic correlation above $T_N$.

The critical temperatures and the critical exponents can be determined from simultaneous fits of $O$ and $\xi$. Unlike bulk Ho, the observed increase of the transverse width is not describable by a simple power-law behavior alone; two characteristic critical regions have been found in all cases. While well above the critical temperature, the data are consistent with a power-law behavior, close to the phase transition the behavior deviates clearly. Figure 5.11 shows analyses using the exponents of the 3D Heisenberg model ($\beta = 0.367$, $\nu = 0.707$) which fits best to both the magnetic order parameter *and* the inverse correlation length. From the combined analysis of the order parameter below the critical temperature and the inverse magnetic correlation length above, ignoring the temperature range close to $T_N$, the critical temperatures were obtained. Although the uncertainties of the single data points do not allow a precise determination of the critical exponents, nearly the same critical temperature $T_N$ was obtained using different critical exponents of different models. This procedure led to the values and error bars of $T_N$ that are given in figure 5.8 of the previous section.

In the temperature interval closer to the critical temperature, there is a smooth change of the width, which is rather describable by an exponential behavior than a power-law-like change of the correlation length. Such an exponential behavior has been found theoretically by Kosterlitz and Thouless for the two-dimensional X-Y model [134, 135]. The correlation length behaves according to the exponential law

$$\xi \propto \exp\left(bt^{-1/2}\right) \quad t > 0, \qquad \xi = \infty \quad t < 0, \tag{5.4}$$

where $t = (T - T_{KT})/T_{KT}$ is the reduced temperature, $T_{KT}$ a characteristic temperature of the system, and $b \approx 1.5$ is a constant [123, 135]. Since the magnetic moments in Ho are confined to the basal planes, the X-Y model may be valid to describe the magnetic properties of ultrathin Ho films near the phase transition. One interesting feature of this model is the fact that the correlation length remains infinite in the ordered phase, which,

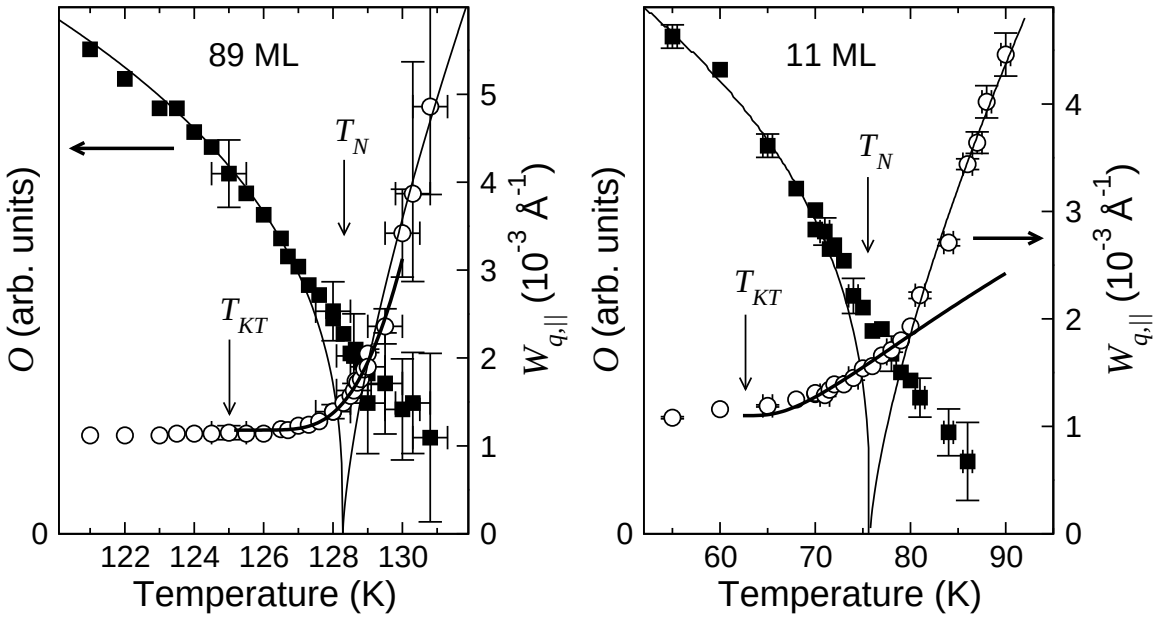


**Figure 5.11:** Square root of the integrated intensity of the magnetic satellite (filled squares) and half width (HWHM) of the transverse scan (open symbols) of an 89-ML and an 11-ML film. The magnetic ordering temperatures $T_N$ were determined by combined power-law fits of both quantities represented by the thin solid lines in the plot. The thick lines represent fits according to equation 5.5, leading to a transition temperature $T_{KT}$.

however, is not observed in the present data and is not expected to be observable in a finite system. A good description of the experimental data can be achieved with a simple modification of the Kosterlitz-Thouless expression, which takes a finite width of the magnetic peak below the ordering temperature into account:

$$W = W^{(0)} + W^{(1)} \exp\left(-1.5 \cdot t^{-1/2}\right), \tag{5.5}$$

where $W^{(1)}$ is a constant and $W^{(0)}$ is the width of the transverse scan below the critical temperature. Indeed, a generalization of the usual scaling hypothesis shows that a finite correlation length at the phase transition may lead to an additive constant to the scaling parameter $W = 1/\xi$ [136, 137]. The results of the fits of equation 5.5 to the experimental data are displayed as the thick lines through the data points above a second transition temperature, denoted as $T_{KT}$. The crossing point of the power-law fit and the fit according to equation 5.5 can be thought of as the transition from the exponential to the power-law behavior. While the described scenario provides a very good description of the experimental data, a final conclusion will probably require a more detailed theoretical modeling.

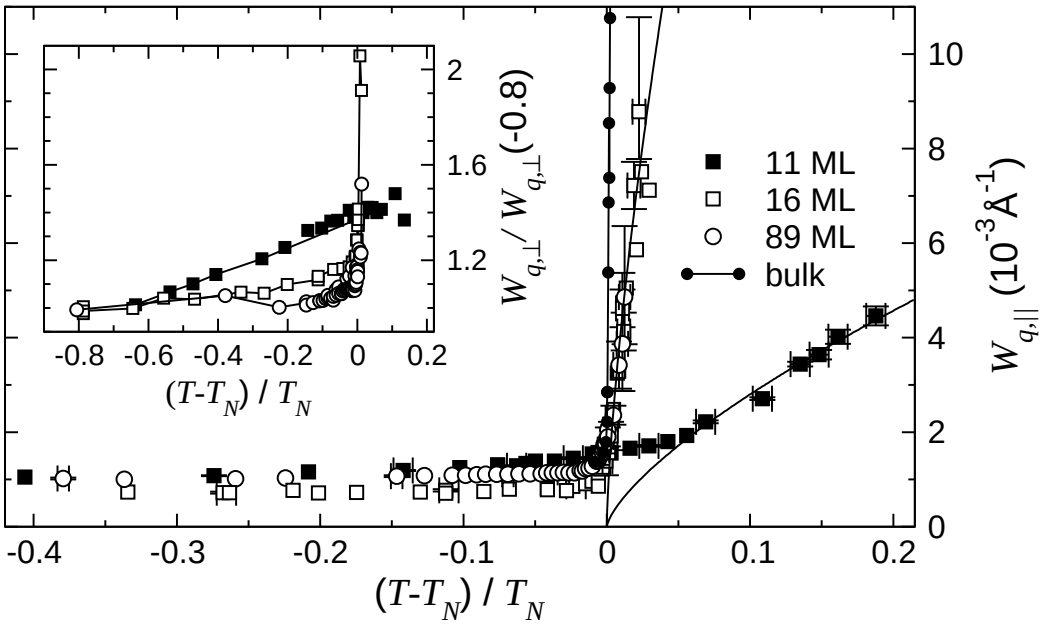


**Figure 5.12:** Comparison of the magnetic satellite widths parallel to the sample surface (transverse width), $W_{q,\parallel}$, of Ho films with different thicknesses as a function of the reduced temperature. The 11-ML film shows an extended interval of short-range magnetic correlations. The data of bulk-Ho metal are from reference 131. The inset shows the satellite widths normal to the sample surface on a reduced scale. The 11-ML film reveals short-range correlation over the whole temperature range.

## Dimensional crossover

As known from theoretical considerations [62,138] and experimental data [26], thin films are often intermediate cases between three- and two-dimensional systems. The dimensionality of magnetic systems is assumed to be determined by the ratio of the temperature-dependent magnetic correlation length, $\xi(T)$, and the film thickness $d$. If these quantities become comparable, a crossover between 3D and 2D behavior may occur [62]. Since $\xi(T)$ shows a strong variation across the phase transition, during which it usually becomes very large, it is likely that a thin film of a given thickness undergoes a dimensional crossover near the critical temperature. A 3D-like behavior far away from the critical temperature, where $\xi(T) \ll d$, may change to a 2D-like behavior near the critical temperature, where the correlation length is increasing ($\xi(T) \gg d$) and becomes limited by the film thickness. Thus, the observed change from the exponential to a power-law-like behavior of the correlation length, as discussed in the previous section, can be interpreted in terms of a temperature-induced dimensional crossover.

As well as a temperature-dependent change of the correlation length can lead to a dimensional crossover, a reduction of the film thickness can do the same, i.e. a thin film can be two-dimensional over the whole temperature range. While the in-plane widths of the 89-ML and 16-ML Ho films show short-range magnetic correlations in an interval of about

3 K above the respective magnetic ordering temperature, this region is extended to about 15 K in case of the 11-ML film. This distinctly different behavior is even more visible, when the peak widths are plotted as a function of the reduced temperature as shown in figure 5.12. The transverse widths of both thicker films (open symbols) show the same behavior with the same slope above $T_N$, which is not much different from the behavior of bulk-Ho metal (solid circles, from reference 131). In contrast to that, a strong change occurs when going to an 11-ML film (solid squares), where the temperature range of short-range correlations is largely extended. Such a behavior is understandable, since it is known that as dimensions are reduced, critical fluctuations and thus short-range correlation become increasingly important [139]. In a two-dimensional, isotropic system critical fluctuations are even strong enough to destroy long-range magnetic order totally [139, 140]. Thus, in a real two-dimensional system, a large temperature interval of short-range magnetic correlation may be expected, while the corresponding three-dimensional system would show long-range magnetic order.

The dimensional crossover as a function of film thickness is also reflected in the diffraction-peak widths normal to the surface, $W_{q,\perp}$. The inset in figure 5.12 shows the longitudinal widths $W_{q,\perp}$ for different films normalized to the respective values at low temperatures. While $W_{q,\perp}$ of the thicker films show qualitatively the same characteristic increase above $T_N$ as the in-plane widths, the 11-ML film does not. It just shows a slow continuous increase of $W_{q,\perp}$, corresponding to a decreasing correlation length within the whole measured temperature interval. Most important, there is no anomaly observable at the phase transition point. This indicates the behavior of a pure two-dimensional magnetic system, with only short-range correlations in the third direction. For the thicker films, the phase transition is observable in all three dimensions.

While even thick films show a two-dimensional behavior in a narrow temperature interval near the phase-transition point, all aspects discussed in this chapter point to a dimensional crossover as a function of thickness in Ho-metal films between 16 and 11 monolayers. This threshold fits well to the period length of the bulk magnetic structure and the thickness interval in which the strongest shift of the critical temperature is observed (figure 5.2). The interval, in which the magnetic structures are strongly altered by the finite sample size, is also theoretically assumed to characterize the inter-dimensional region [138]. Since there is an offset $d_0$ in the finite-size scaling of AFM systems, as shown in the previous section, it is likely that the relevant thickness scale is determined by the magnetic period length.

## $c-$axis lattice parameter

An interesting and rarely studied aspect of magnetic systems is the influence of magnetic short-range correlation on other properties of the system, e.g. on the thermal lattice expansion due to the strong coupling of the magnetic to the crystalline structure. Ultrathin films are especially suited for this study because of the extended temperature interval of short-range magnetic correlations.

Due to the strong magneto-elastic coupling in lanthanide metals, magnetic proper-

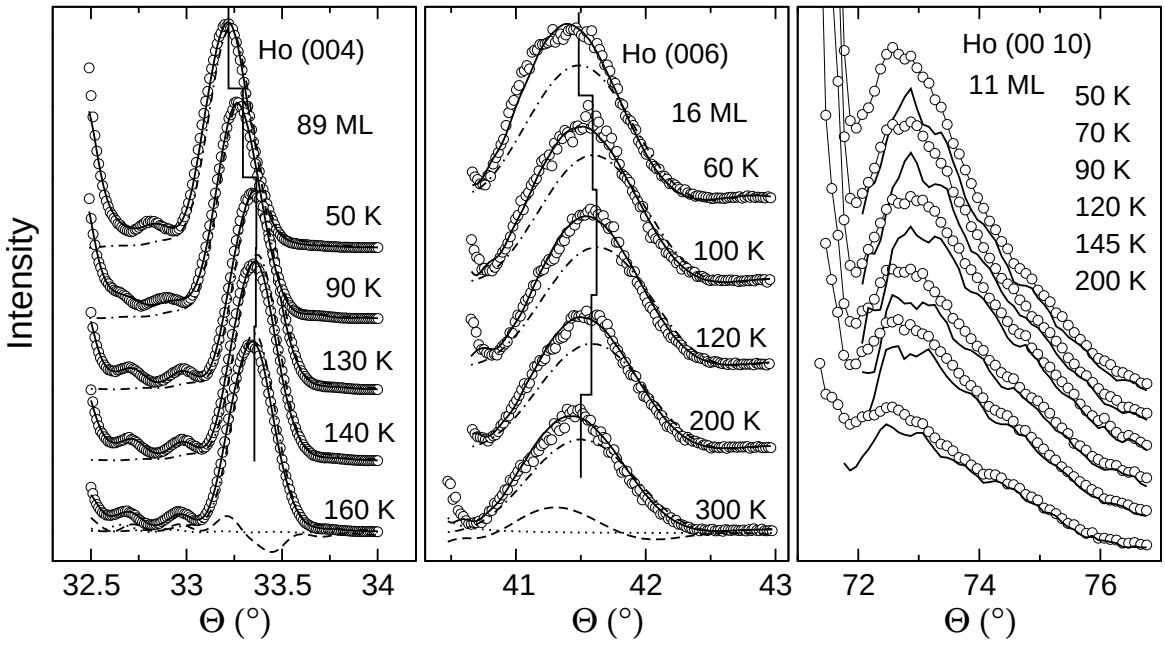


**Figure 5.13:** Bragg peaks of Ho thin films embedded between Y layers recorded with 8- to 10-keV photons. From left to right: (004) reflections from an 89-ML, (006) reflections from a 16-ML, and (00 10) reflections from an 11-ML film at various temperatures. The solid lines through the data points in the left and middle panel are the results of least-squares fit analyses. The subspectra represent the contributions of the Ho (dash-dotted) and the Y Bragg peak (dotted) plus an interference term (dashed line). The solid lines below the spectra in the rightmost panel are the residual intensities after subtracting the Y contribution.

ties are reflected in the temperature dependence of the lattice parameters. In the helical AFM phase, the $c-$axis lattice parameter of bulk Ho exhibits an anomalous expansion with decreasing temperature, whereas the $a-$ and $b-$axis parameters get more and more compressed. Above $T_N$, where no magnetic long-range order is present, a normal thermal expansion takes place. As a result, there is a characteristic minimum in the $c-$axis lattice parameter that is connected with the disappearance of the long-range magnetic order at the critical phase transition point, $T_N$. While in the bulk the magnetic order vanishes in a narrow temperature interval, in ultrathin films, the region of short-range magnetic correlation above the ordering temperature is largely extended as discussed in the previous section. Therefore the two characteristic temperatures, the ordering temperature and the temperature at which also the short-range magnetic order disappears, are different. If short-range magnetic correlations are present over an extended temperature interval, both temperatures can be clearly separated, which allows us to study the influence of the magnetic correlation length on the crystalline lattice.

The $c-$axis lattice parameters of the MBE-grown samples have been studied by means of conventional x-ray diffraction using photon energies between 8 and 10 keV. Scattering

from thin films and especially from layered systems suffers from similar difficulties as those encountered in the analysis of magnetic peaks in the previous chapters. The increasing width of the diffraction peaks with decreasing thickness of the Ho layers can lead to an overlap of the Bragg peaks of different components. Especially the Y Bragg peaks lie very close to the Ho peaks, because the Y $c-$axis parameter differs from that of Ho by only 2 percent. To separate the contributions of Ho and Y, higher-order Bragg peaks were measured. Figure 5.13 shows data of the (004) Bragg peak of the 89-ML, the (006) Bragg peak of the 16-ML, and the (00 10) Bragg peak of the 11-ML film at various temperatures. In case of the two thicker films, a fit analysis could be applied to obtain the lattice parameters. The analysis takes the structure factor of the Ho slab and of the two Y slabs according to equation 2.6 into account plus an interference term. The solid lines through the data points in the left and middle panel represent the results of the least-squares fit analyses. The subspectra corresponding to the mentioned contributions are shown for the respective lowest spectra. In case of the 11-ML film even the (00 10) Bragg peak is only a weak shoulder of the dominating Y Bragg peak, and a fit analysis as applied to the other data is not reliable. For this sample, the temperature dependence of the lattice parameter was obtained by analyzing the change of the center of mass of the Ho signal. For this purpose, the dominating Y Bragg peak was described by a least-squares fit, and the obtained Y contribution was subtracted from the spectrum. The resulting Ho contribution is displayed as a thick solid line below each spectrum in the right panel of figure 5.13. The center of mass is not necessarily identical to the Bragg-peak position, and thus it is not possible to extract the absolute values of the lattice parameter from this analysis, but the change of the center of mass reflects the relative change of $c$. To test this method, it was also applied to the 16-ML film. Both methods, the least-squares fit analysis and the change of the center of mass led to the same results for this film.

Figure 5.14 shows the changes of the $c-$axis lattice parameters of the three films with different thicknesses (right panels) and compares them with the critical-scattering data recorded from the respective magnetic-superstructure satellites (left panels), as discussed in the previous sections. The gray bars in all panels mark the temperature interval in which short-range magnetic correlations have been observed. Except for the reduced ordering temperature, the lattice parameters of both thicker films exhibit the same behavior similar to that of bulk samples. While $T_N$ of the thick film is still too close to the bulk value to see an effect, the minimum in the lattice parameter of the 16-ML film is clearly shifted towards the reduced Néel temperature. How the observed and characteristic minimum is connected with the critical regime of the phase transition cannot be resolved for the two thicker films. But it is readily possible in case of the 11-ML film. The data clearly reveal that there are magnetostrictive effects in the presence of only short-range magnetic correlations, and the minimum in the $c-$axis lattice parameter is not related to the disappearance of long-range magnetic order at $T_N$, but occurs at a higher temperature when the *short-range* magnetic order disappears.

One may speculate about the reason why the observed anomalous lattice expansion sets in already in the presence of short-range magnetic order. The $c-$axis expansion towards lower temperatures arises from the dominant exchange magnetostriction discussed

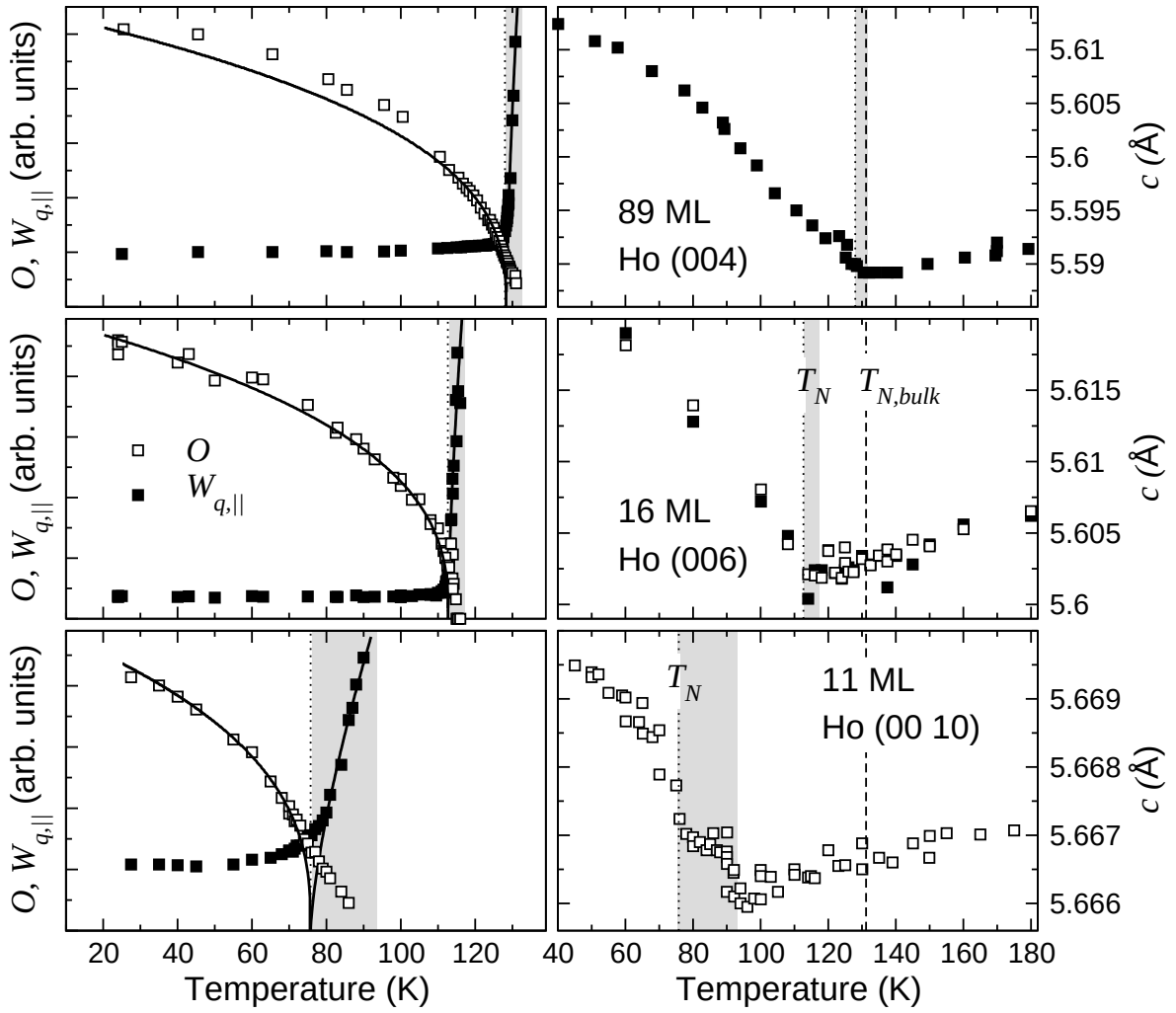


**Figure 5.14:** Left panels: half width $W_{q,\|}$ of the rocking scans (filled symbols) and square-root of the integrated intensities (open symbols) obtained from the (000+$\tau$) magnetic satellite of an 89-ML (top), 16-ML (middle), and 11-ML (bottom) film as a function of temperature. The solid lines through the data points are the results of power-law fits. Right panels: the corresponding $c-$axis parameters as obtained from the analysis of the data in figure 5.13. The gray bars show the temperature interval in which short-range magnetic correlations were observed. Filled symbols in the right panels denote the results of least-squares fits, open symbols those obtained by a center-of-mass analysis.

in chapter 1. The relative change $\Delta c/c$ due to this contribution is usually regarded as proportional to the square of the sublattice magnetization (equation 1.2). But even in the presence of short-range magnetic correlations the fluctuating domains are a few hundred Å in size, which is more than any magnetic interaction length. Apparently, these short-range correlations are sufficient to stabilize magnetostriction; maybe the different time scales for magnetic fluctuations and lattice motions play a role here. In that scenario, the minimum

in the temperature dependence of the lattice parameter would not be related to the disappearance of long-range magnetic order, but would occur at a temperature, where magnetic correlations on a short range vanish as indicated by the disappearance of the satellite.